ETMM8: 8th International ERCOFTAC Symposium on
Engineering Turbulence Modelling and Measurements
9–11 June 2010, Marseille, France

A LOW REYNOLDS NUMBER PARTIALLY-AVERAGED NAVIER-STOKES MODEL FOR TURBULENCE

J.M. Ma[1,2], *S.-H. Peng*[2,3], *L. Davidson*[2] *and F. Wang*[1]

[1] *China Agricultural University, Beijing, China*
[2] *Chalmers University of Technology, Gothenburg, Sweden*
[3] *Swedish Defence Research Agency (FOI), Stockholm, Sweden*

jiameima@gmail.com, peng@foi.se, lada@chalmers.se, wangfj@cau.edu.cn

Abstract

A low Reynolds number (LRN) formulation based on the Partially Averaged Navier-Stokes (PANS) modelling method is presented, which incorporates improved asymptotic representation in near-wall turbulence modelling. The effect of near-wall viscous damping is thus better accounted for in simulations of wall-bounded turbulent flows. The proposed LRN PANS model uses an LRN $k-\varepsilon$ model as the base model and introduces its model functions into the PANS formulation. As a result, the inappropriate wall-limiting behavior inherent in the original PANS model is corrected. The proposed LRN PANS model is scrutinized in computations of turbulent channel flow and periodic hill flow. In comparison with available DNS or LES data, the LRN PANS model has produced better predictions than the original PANS model, particularly in the near-wall region and for resolved turbulence statistics.

1 Introduction

In spite of robust turbulence-resolving capabilities, it is well known that the use of Large Eddy Simulation (LES) has often been limited to turbulent flows at relatively low Reynolds numbers due to its prohibitively high requirement on computing resources in simulations of realistic engineering flows at high Reynolds numbers. This has thus motivated intensive studies of hybrid RANS-LES methods, e.g. Detached Eddy Simulation (DES) by Spalart et al. (1997), Scale-Adaptive Simulation (SAS) by Menter (2003) and Partially-Averaged Navier-Stokes (PANS) model by Girimaji (2006).

The PANS model was developed with an intention to smoothly simulate turbulent flows using a hierarchic rank of modelling approaches from RANS to Direct Numerical Simulation (DNS) (Girimaji, 2006). Different cases were studied using the PANS model, for example, flow over a square cylinder (Girimaji, 2006), cavity flow (Basu et al., 2007), a turbulent square jet (Girimaji and Lavin, 2007) and so on. The derivation of the original PANS model has been stemmed from the standard RANS $k-\varepsilon$ model (Girimaji, 2006). It is well known that in the context of RANS modelling it is highly inappropriate to directly integrate the standard $k-\varepsilon$ model to the wall surface. This drawback is inherited by the resulting PANS model equations, however. On the other hand, LRN RANS models usually employ empirical damping functions in the model equations, which ensure that the viscous stresses take over turbulent Reynolds stresses at low Reynolds numbers and in the viscous sublayer adjacent to solid walls. There exist a number of LRN RANS models stemmed from the $k-\varepsilon$ models. Of the existing LRN $k-\varepsilon$ models, the LRN model by Abe et al. (1994) (hereafter the AKN model) has shown reasonable performance in modelling different flows. The AKN model is an improved version of the LRN $k-\varepsilon$ model by Nagano and Tagawa (1990), using the Kolmogorov velocity scale, $u_\varepsilon \equiv (\nu\varepsilon)^{1/4}$, in the damping function.

This work presents an LRN variant of the PANS model using the LRN AKN $k-\varepsilon$ model as the base model. The model coefficients are modified in order to account for near-wall turbulence. The proposed model is examined in simulations of fully developed turbulent flows in a clean channel and in a channel with hills mounted periodically on the bottom wall.

In what follows, the modelling formulation are presented in Section 2. In Section 3 the numerical methods used in the computations are briefly introduced. The results are then presented and discussed in Section 4, and the conclusions are drawn in Section 5.

2 Modelling formulation

For incompressible turbulent flows, the partial averaging to the governing equations gives

$$\frac{\partial \bar{u}_i}{\partial x_i} = 0 \tag{1}$$

$$\frac{\partial \bar{u}_i}{\partial t} + \frac{\partial (\bar{u}_i \bar{u}_j)}{\partial x_j} = -\frac{1}{\rho}\frac{\partial \bar{p}}{\partial x_i} + \frac{\partial}{\partial x_j}\left(\nu \frac{\partial \bar{u}_i}{\partial x_j} - \tau_{ij}\right)$$

where τ_{ij} is the central second moment resulting from the partial averaging for the nonlinear terms, and $\tau_{ij} = (\mathcal{P}(U_i U_j) - \bar{u}_i \bar{u}_j)$, where $\mathcal{P}$ denotes the partial-averaging operator and U_i indicates instantaneous velocity components. This term is similar to

the Reynolds stress tensor in the RANS equations or to the subgrid-scale (SGS) stress tensor after the spatial filtering in the LES equations. For simplicity, we have used the terminology of Reynolds stresses for τ_{ij} in Eq. (1).

In order to formulate the PANS eddy viscosity, Girimaji (2006) defined another two quantities, the partially-averaged turbulent kinetic energy, k_u and its dissipation rate ε_u, so that $\nu_u = C_\mu k_u^2/\varepsilon_u$. In the derivation of the transport equations for k_u and ε_u, two parameters, f_k and f_ε, have been introduced, relating the unresolved small scales to the resolved fluctuating scales. Parameter f_k defines the ratio of unresolved (partially-averaged) turbulent kinetic energy (k_u) to the total kinetic energy (k), and f_ε is the ratio between the unresolved (ε_u) and the total (ε) dissipation rates. These give

$$k = k_u/f_k \text{ and } \varepsilon = \varepsilon_u/f_\varepsilon \tag{2}$$

The extent of the resolved part is now determined by f_k and f_ε. In his PANS derivation, Girimaji (2006) employed the standard $k-\varepsilon$ model as the base model. The resulting model is thus termed here the *Standard PANS* model. Below, we re-formulate the PANS model based on an LRN $k-\varepsilon$ model in order to attain improved near-wall asymptotic behavior. Incorporating empirical damping functions, a LRN $k-\varepsilon$ RANS model can often be cast in a general form, the equations can be written as

$$\begin{aligned}
\frac{\partial k}{\partial t} + \frac{\partial (k\bar{U}_j)}{\partial x_j} &= \frac{\partial}{\partial x_j}\left[\left(\nu + \frac{\nu_t}{\sigma_k}\right)\frac{\partial k}{\partial x_j}\right] \\
&\quad + P_k - \varepsilon \\
\frac{\partial \varepsilon}{\partial t} + \frac{\partial (\varepsilon\bar{U}_j)}{\partial x_j} &= \frac{\partial}{\partial x_j}\left[\left(\nu + \frac{\nu_t}{\sigma_\varepsilon}\right)\frac{\partial \varepsilon}{\partial x_j}\right] \\
&\quad + C_{\varepsilon 1} f_1 P_k \frac{\varepsilon}{k} - C_{\varepsilon 2} f_2 \frac{\varepsilon^2}{k} \\
\nu_t &= C_\mu f_\mu \frac{k^2}{\varepsilon}
\end{aligned} \tag{3}$$

In Eq. (3), ν_t is RANS eddy viscosity, f_1, f_2 and f_μ are additional damping function that have usually been employed to correct the near-wall asymptotic properties in the modelling. Moreover, it should be noted that the RANS mean velocity field is denoted by $\bar{U}_i$ in these equations. As indicated by Girimaji (2006), one should have $\bar{U}_i = \langle \bar{u}_i \rangle$, with the angular brackets indicating the time-averaged flow quantities.

Using the same damping function, f_μ, as for the LRN model, the PANS turbulent viscosity, ν_u, in the LRN PANS model is defined in terms of k_u and ε_u, viz.

$$\nu_u = C_\mu f_\mu \frac{k_u^2}{\varepsilon_u} \tag{4}$$

In the derivation of the k_u and ε_u equations for the LRN PANS model, the same procedure has been invoked as for the standard PANS paradigm (Girimaji, 2006). Parameters f_k and f_ε have also been assumed to be constants. Without repeating all the details of the PANS formulation, as discussed in Girimaji (2006), we directly write the resulting transport equation for k_u in the LRN PANS model, which takes the same form as in the standard PANS model. This gives

$$\frac{\partial k_u}{\partial t} + \frac{\partial (k_u \bar{u}_j)}{\partial x_j} = \frac{\partial}{\partial x_j}\left[\left(\nu + \frac{\nu_u}{\sigma_{ku}}\right)\frac{\partial k_u}{\partial x_j}\right] + (P_u - \varepsilon_u) \tag{5}$$

where $\sigma_{ku} = \sigma_k f_k^2/f_\varepsilon$, and the production term, P_u, is expressed in terms of the PANS eddy viscosity, ν_u, and the strain rate of PANS-resolved flow field, viz.

$$P_u = \nu_u \left(\frac{\partial \bar{u}_i}{\partial x_j} + \frac{\partial \bar{u}_j}{\partial x_i}\right)\frac{\partial \bar{u}_i}{\partial x_j} \tag{6}$$

Note that, in deriving Eq. (5), a relation of $P_u - \varepsilon_u = f_k(P_k - \varepsilon)$ is implied (Girimaji, 2006). With $\varepsilon = \varepsilon_u/f_\varepsilon$, this relation can be re-written as

$$P_k = \frac{1}{f_k}(P_u - \varepsilon_u) + \frac{\varepsilon_u}{f_\varepsilon} \tag{7}$$

Equation (7) was exploited to derive the ε_u equation in the PANS model. With an LRN model as the base model, the ε equation may invoke model functions, f_1 and f_2, respectively, in the production and destruction terms, which are kept in the related model coefficient for the resulting ε_u equation. This has led to the following expression.

$$\begin{aligned}
&\frac{\partial \varepsilon_u}{\partial t} + \frac{\partial (\varepsilon_u \bar{u}_j)}{\partial x_j} = f_\varepsilon \left[\frac{\partial \varepsilon}{\partial t} + \frac{\partial (\varepsilon \bar{u}_j)}{\partial x_j}\right] \\
&= f_\varepsilon \left\{\frac{\partial}{\partial x_j}\left[\left(\nu + \frac{\nu_t}{\sigma_\varepsilon}\right)\frac{\partial \varepsilon}{\partial x_j}\right] + C_{\varepsilon 1} f_1 P_k \frac{\varepsilon}{k} - C_{\varepsilon 2} f_2 \frac{\varepsilon^2}{k}\right\}
\end{aligned} \tag{8}$$

In order to close the ε_u equation in the LRN PANS model, the relations of $\varepsilon = \varepsilon_u/f_\varepsilon$ and $k = k_u/f_k$ are introduced into Eq. (8). The resulting ε_u equation in the LRN PANS model takes the following form.

$$\begin{aligned}
\frac{\partial \varepsilon_u}{\partial t} + \frac{\partial (\varepsilon_u \bar{u}_j)}{\partial x_j} &= \frac{\partial}{\partial x_j}\left[\left(\nu + \frac{\nu_u}{\sigma_{\varepsilon u}}\right)\frac{\partial \varepsilon_u}{\partial x_j}\right] \\
&\quad + C_{\varepsilon 1} f_1 P_u \frac{\varepsilon_u}{k_u} - C_{\varepsilon 2}^* \frac{\varepsilon_u^2}{k_u}
\end{aligned} \tag{9}$$

where $\sigma_{\varepsilon u} = \sigma_\varepsilon f_k^2/f_\varepsilon$. Note that the LRN model functions, f_1 and f_2, enter into the model coefficient, $C_{\varepsilon 2}^*$, in the relation of

$$C_{\varepsilon 2}^* = C_{\varepsilon 1} f_1 + \frac{f_k}{f_\varepsilon}(C_{\varepsilon 2} f_2 - C_{\varepsilon 1} f_1) \tag{10}$$

Equations (4), (5) and (9) form the proposed PANS formulation based on an LRN $k-\varepsilon$ model. Obviously, many existing LRN $k-\varepsilon$ models in the context of RANS complies with the formulation towards a LRN PANS model. In the present work, we have adopted the AKN LRN $k-\varepsilon$ model (Abe et al., 1994). The model constants in the LRN PANS formulation

thus take the following values: $C_{\varepsilon 1} = 1.5, C_{\varepsilon 2} = 1.9, \sigma_k = 1.4, \sigma_\varepsilon = 1.4, C_\mu = 0.09$. With the AKN LRN $k-\varepsilon$ model, note that $f_1 = 1$ and the other two model functions, f_2 and f_μ, hold the following forms, respectively,

$$f_\mu = \Big[1 - \exp\Big(-\frac{y^*}{14}\Big)\Big]^2 \Big\{1 + \frac{5}{R_t^{3/4}} \exp\Big[-\Big(\frac{R_t}{200}\Big)^2\Big]\Big\}$$
$$f_2 = \Big[1 - \exp\Big(-\frac{y^*}{3.1}\Big)\Big]^2 \Big\{1 - 0.3\exp\Big[-\Big(\frac{R_t}{6.5}\Big)^2\Big]\Big\} \quad (11)$$

Variables, R_t and y^*, are defined in terms of k_u and ε_u for the LRN PANS model. These are

$$R_t = \frac{k_u^2}{\nu \varepsilon_u} \text{ and } y^* = \frac{V_\varepsilon y}{\nu} \text{ with } V_\varepsilon = (\varepsilon_u \nu)^{1/4} \quad (12)$$

3 Computational set-up

An incompressible, finite volume code was used (Davidson and Peng, 2003). The second-order central differencing scheme was used for spatial discretization of all terms except for the convection terms in the k_u and ε_u equations, for which a hybrid central/upwind scheme was employed. The temporal advancement was approximated using the second-order Crank-Nicolson scheme. The numerical procedure was based on an implicit, fractional step technique with a multigrid pressure Poisson solver (Emvin, 1997) and a non-staggered grid arrangement.

Two different flow configurations were computed with the new model. For comparison, the standard PANS model was also employed in the computations.

The first test case is a fully-developed channel flow. Note that previous PANS simulations have usually been conducted for bluff-body flows. The test case is selected to highlight the feasibility of the PANS model in computations of attached boundary layer flows, particularly, the modelling behavior in representing near-wall turbulence. Two different Reynolds numbers, $Re_\tau = 550$ and 950, based on the friction velocity, u_τ, and half of the channel height, $\delta = y_{max}/2$, were considered. The computational domain has the dimensions of $x_{max} = 3.2$, $y_{max} = 2.0$ and $z_{max} = 1.6$. For both Reynolds numbers, a $64 \times 80 \times 64$ mesh was used in the streamwise (x), wall-normal (y) and spanwise (z) directions, respectively. With this grid, the first near-wall node is located at $y^+ = 0.36$ for $Re_\tau = 550$ and $y^+ = 0.62$ for $Re_\tau = 950$. The time step was set to $\Delta t = 6.25 \times 10^{-4}$ for both Reynolds numbers. DNS data were taken from the work by Hoyas and Jimenez (2008).

The second test case concerns flow separation in a channel with periodic hills mounted on the bottom wall in the streamwise direction. The periodic hill flow is characterized by turbulent flow separation, recirculation, reattachment and acceleration phenomena. The computational domain starts from one hill crest and extends to the next, separated by a distance of $L = 9h$. The upper and lower sides are bounded by plane and curved wall surfaces, respectively. The extension in the spanwise direction is $L_z = 4.5h$. The computational mesh consists of $N_x \times N_y \times N_z = 160 \times 80 \times 32$ cells in the streamwise, wall-normal and spanwise directions, respectively. The Reynolds number, based on the hill height, h, and the bulk velocity, U_b, above the hill crest is $Re_b = U_b h/\nu = 10595$. The time step was set to $\Delta t = 6.0 \times 10^{-3}$. After 20 flow-through times, statistical analysis was made over a time period of another 20 flow-through times. The results were also averaged in space over the spanwise direction.

For both test cases, no-slip conditions were specified on the walls for the velocity components. The values of k_u and ε_u on the wall surface were set by $k_{u,w} = 0$ and $\varepsilon_{u,w} = 2\nu k_{u,1}/y_1^2$, respectively, where $k_{u,1}$ is the value of k_u at the first near-wall node and y_1 is the wall distance of this node. Periodic boundary conditions were imposed on the streamwise and spanwise boundaries.

4 Results and discussion

Channel flow

The following values were tested for f_k in the simulation of channel flow, namely, $f_k = 0.1$, 0.3, 0.4, 0.5, 0.6 and 1.0. With the current grid for the channel flow, it was found that, for $f_k \leq 0.3$, the model plays an insignificant role in the simulation, that is, the value of ν_u becomes negatively small. In the following discussion, only the results computed with $f_k = 0.4$, 0.5 and 1.0 are presented.

Figure 1 compares the mean streamwise velocities, computed using the standard PANS model and the proposed LRN PANS model with the DNS data (Hoyas and Jimenez, 2008) for both $Re_\tau = 550$ and $Re_\tau = 950$. It was found that, for $f_k = 1.0$, the computations give steady RANS solutions. The LRN PANS model returns to the AKN LRN $k-\varepsilon$ model, while the standard PANS model becomes identical to the standard $k-\varepsilon$ model. This has also been reflected in the predictions, as illustrated in Fig. 1 with $f_k = 1.0$. The reason for the poor prediction by the standard $k-\varepsilon$ model is due to the fact that a low Reynolds number grid is highly inappropriate to accommodate the high Reynolds number model.

With a reduced value of f_k, the PANS formulation makes the modelling shift away from a RANS computation and come closer to LES with increasingly resolved turbulent contents. This is demonstrated by the results computed using $f_k = 0.4$ and $f_k = 0.5$, as shown in Fig. 1. The LRN PANS model is able to give a generally improved tendency of the profile, in spite of the over-prediction in the logarithmic layer. The improvement is particularly obvious in the viscous sublayer, thanks to the correct asymptotic properties in-

herent in the LRN PANS formulation. Using $f_k = 0.4$, the standard PANS and the LRN PANS models have produced very similar results for $Re_\tau = 550$ and $Re_\tau = 950$, which are in reasonable agreement with the DNS data.

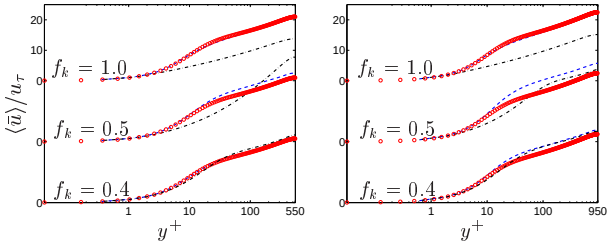

(a) $Re_\tau = 550$ (b) $Re_\tau = 950$

Figure 1: Channel flow. Streamwise velocity. ---: LRN PANS model; ---: standard PANS model; ○: DNS data.

In the computations, it was found that $f_k = 0.4$ gives the best predictions for both the standard and the LRN PANS models. To highlight the modelling performance for near-wall turbulence, the results computed with $f_k = 0.4$ are presented below for the turbulence statistics.

In Figure 2 the PANS-resolved Reynolds normal stresses are compared to DNS data. It is shown that, at $Re_\tau = 550$, the resolved turbulent fluctuations computed with the LRN PANS model are nearly identical to the DNS data, and are in reasonable agreement at $Re_\tau = 950$. In general, the LRN model has shown better performance than the standard model. This is particularly true in the vicinity of the wall surface over the viscous sublayer for $y^+ \leq 10$.

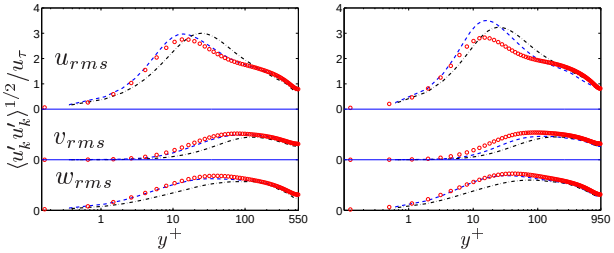

(a) $Re_\tau = 550$ (b) $Re_\tau = 950$

Figure 2: Channel flows. PANS-resolved turbulent normal stresses with $f_k = 0.4$. ---: LRN PANS model; - - -: standard PANS model; ○: DNS data. No summation in $\langle u_k' u_k' \rangle$ for the $y-$axis.

Figure 3 further shows the resolved Reynolds shear stress, $-\langle u'v' \rangle$, with $f_k = 0.4$ in comparison with DNS data. The under-estimation in $-\langle u'v' \rangle$ is large for the standard PANS model in the viscous sublayer and up to $y^+ \approx 30$, whereas the prediction was greatly improved by the LRN model for both $Re_\tau = 550$ and $Re_\tau = 950$.

The under-prediction of resolved Reynolds stresses by the standard PANS model is closely associated to large values of the modelled eddy viscosity in the near-wall region. The results, as illustrated in Figs. 2 and 3, show that the LRN formulation indeed introduces correct wall-limiting behavior into the modelling. It is also demonstrated that correct near-wall asymptotic modelling improves the predictions of resolved turbulence statistics.

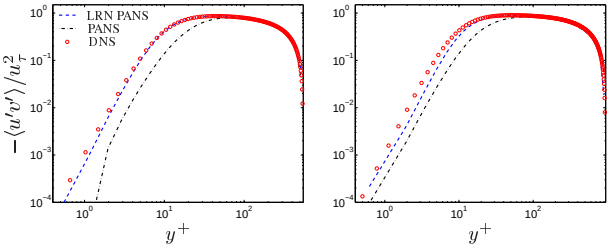

(a) $Re_\tau = 550$ (b) $Re_\tau = 950$

Figure 3: Channel flows. PANS-resolved turbulent shear stress. $f_k = 0.4$.

Periodic hill flow

The periodic hill flow was computed to verify PANS performance in modelling turbulent flow separation and reattachment. For this test case, the simulation is compared with a wall-resolved LES (Fröhlich et al., 2005). It is noted here that the present grid, with $160 \times 80 \times 32$ cells in a domain of $9h \times 3.035h \times 4.5h$, is much coarser than the wall-resolved LES mesh, which uses $196 \times 128 \times 186$ cells in a domain of $9h \times 3.035h \times 9h$. In view of the grid resolution, the PANS modelling in the present work lies thus in between RANS modelling and wall-resolved LES. It is expected that the performance of the PANS modelling should be similar to a hybrid RANS-LES model.

Using the same mesh, a number of computations were conducted using various values of f_k, with $f_k = 0.4, 0.5, 0.6, 0.8$ and 1.0. In comparison with the LES result, it was found that the PANS computation with $f_k = 0.4$, using either the standard or the LRN model, produced the best prediction of the separation bubble on the rear side of the hill in terms of the locations of both the separation and the reattachment.

The locations of flow separation and reattachment, x_s and x_r, respectively, are plotted in Fig.4 (a) and (b) as function of f_k. As seen, the LRN PANS model produces accurate predictions of x_s and x_r with $f_k = 0.4$, whereas the standard PANS model shows a somewhat earlier flow separation and the reattachment is slightly delayed. With increasing values of f_k, the location of flow separation is shifted downwards along the lee-side of the hill, and the reattachment location is first delayed and then moves back toward the hill foot. With $f_k = 1.0$, both models produce overall attached flow over the hill and between the hills, namely, $x_s = x_r = 0$. It should be noted that, with $f_k = 1.0$, both models return to their respective RANS base models, giving steady solutions based on the standard $k - \varepsilon$ model and the AKN LRN $k - \varepsilon$ model.

The following presentation presents only the computations obtained with $f_k = 0.4$, for which both the

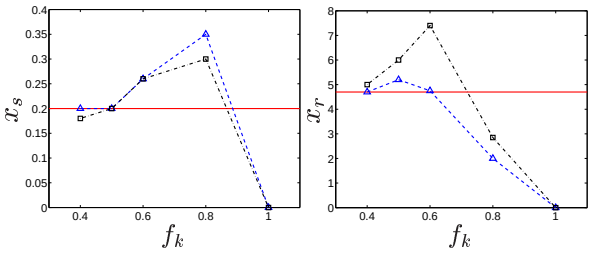

(a) Separated locations (b) Reattached locations

Figure 4: Periodic hill flow: Locations of separation and reattachment, x_s and x_r, versus parameter f_k used in PANS computations. Standard PANS gives $x_s \approx 0.18$ and $x_r \approx 5.0$, and LRN PANS gives $x_s \approx 0.2$ and $x_r \approx 4.7$ with $f_k = 0.4$, compared to the LES data ($x_s^{LES} = 0.2$ and $x_r^{LES} = 4.7$. △: LRN PANS; □: standard PANS; —— : LES data.

standard and the LRN models have produced the best predictions in comparison with the LES data. The profiles were extracted at locations of $x = 0.05h$, $2.0h$, $6.0h$ and $8.0h$, respectively.

The mean velocity profiles are presented in Fig. 5 in comparison with the LES data. It is shown that both the standard and the LRN PANS models have produced very reasonable predictions, but some relatively large discrepancies are observed in the prediction by the standard model. Near the lower wall, as well as in the free shear layer (at $x = 2.0h$), the standard PANS has somewhat over-predicted both $\langle\bar{u}\rangle$ and $\langle\bar{v}\rangle$.

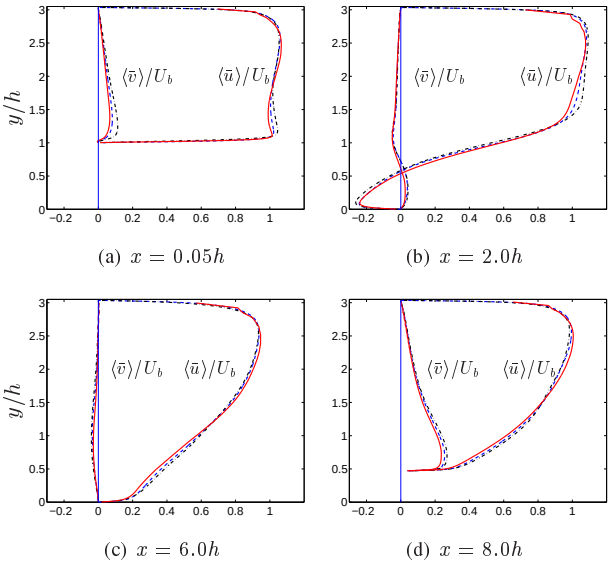

(a) $x = 0.05h$ (b) $x = 2.0h$

(c) $x = 6.0h$ (d) $x = 8.0h$

Figure 5: Comparison of mean velocities between PANS and LRN PANS models. - - - : LRN PANS model; - - - : standard PANS model; —— : LES data.

Figure 6 plots the distributions of the resolved Reynolds stresses by the standard and LRN PANS models in comparison with the LES data. It is shown that, at $x = 0.05h$ before the separation occurs, the proposed LRN model gives very good predictions for both the streamwise and spanwise fluctuations near the wall, whereas the standard model over-predicts the near-wall peaks of $\langle u'u'\rangle$ and $\langle w'w'\rangle$. Both models under-estimate $\langle v'v'\rangle$ near the wall. In the recirculation region (at $x = 2.0h$), the resolved streamwise fluctuation is over-estimated around the peak at $y/h \approx 1$ by both models. While the LRN model presents better predictions for $\langle u'u'\rangle$ over the recirculation bubble at $x = 2.0h$, the distribution of $\langle v'v'\rangle$ is closer to the LES data as given by the standard model in the free shear layer above the bubble. After the reattachment of the separation bubble, at $x = 6.0h$ and $x = 8.0h$, the LRN model produces generally better or similar predictions, as compared to the standard PANS model. For $\langle u'u'\rangle$ and $\langle w'w'\rangle$, the LRN model has indeed rendered improved distributions in the attached boundary layer near the top and bottom walls and even in the near-wall reverse flow of the recirculation region (e.g. at $x = 2.0h$). However, both models have under-estimated $\langle v'v'\rangle$ close to the wall surface. This might be related partly to the grid resolution in the wall layer, which is much coarser than in wall-resolved LES, and hence the near-wall sweep and ejection phenomena are not sufficiently resolved by the PANS simulations. For the resolved turbulent shear stress, $\langle u'v'\rangle$, the improvement over the standard PANS model in the predictions by the LRN model is obvious, particularly in the recirculation region and in the free shear layer. Near the top wall, $\langle u'v'\rangle$ is under-predicted. Although not shown here, nonetheless, the total turbulent shear stress becomes closer to the LES data by including the modelled part.

5 Conclusions

A low Reynolds number PANS formulation is presented, which is able to improve the near-wall modelling behavior of the standard PANS model. The formulation follows a procedure same as to reach the original PANS model but has been based on a general low Reynolds number $k - \varepsilon$ form with additional empirical model functions. The resulting PANS formulation can thus use any existing LRN $k - \varepsilon$ model as the base model to form an LRN PANS variant. In the present work, the AKN LRN model has been taken as the platform in the verification of the LRN modelling performance, in which two damping functions have thus been incorporated.

Computations were made for two test cases, including turbulent channel flow and periodic hill flow. One of the main purposes has been to investigate the capabilities of PANS modelling in predicting both attached and separated flows. With the same grid resolution for each test case, the effect of the PANS modelling parameter, f_k, was also investigated. The results, computed by both the (original) standard and the proposed LRN PANS models, have been discussed in comparison with available DNS or LES data.

For the channel flow computations, it is shown that the LRN PANS model is able to produce improved

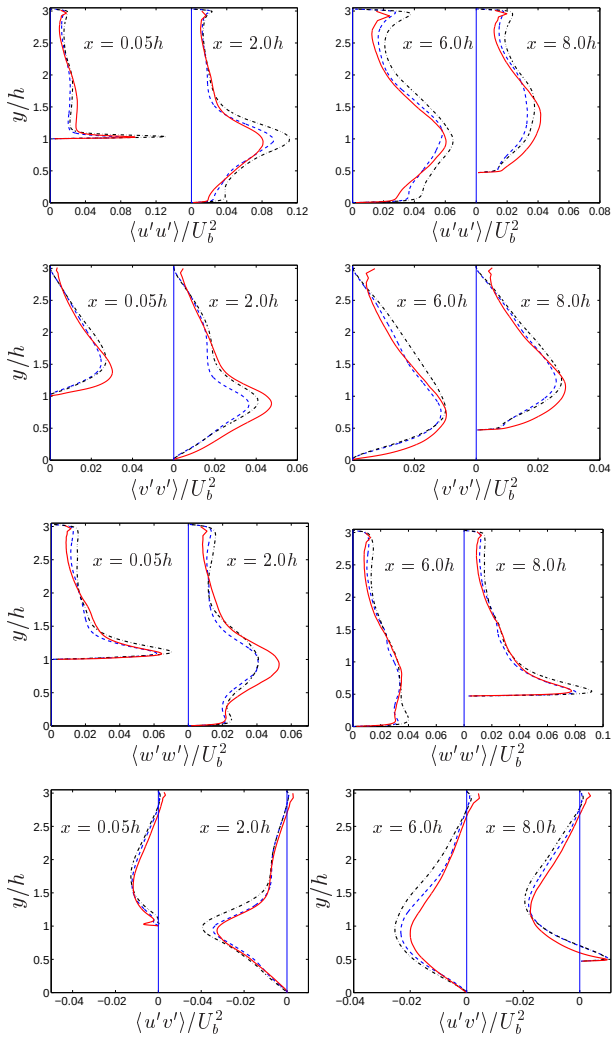

Figure 6: Periodic hill flow: Profiles of resolved Reynolds stresses. - - -: LRN PANS model; - - -: standard PANS model; ——: LES data.

predictions for both the mean flow velocity and the resolved turbulence statistics. The model also demonstrates a reasonable response to the change of parameter f_k. In contrast to the inappropriate wall-limiting behavior inherent in the standard PANS model, the LRN formulation corrects the asymptotic properties of the modelled turbulence quantities, which have consequently enabled improved predictions of resolved turbulence statistics in the wall layer.

The function of the PANS method is well demonstrated for the hill flow, with a much coarser grid in comparison with a wall-resolved LES. Both the standard and the LRN PANS models produce reasonable predictions for the mean flow and the resolved turbulent quantities. Nonetheless, the improvement due to the LRN formulation is sensible. The LRN formulation has rendered generally better predictions in near-wall regions than the standard PANS model. Both models produce similar predictions for the resolved wall-normal fluctuation, which is however under-estimated near the wall in comparison with the LES data.

Acknowledgments

The first author was supported by the China Scholarship Council, the Beijing Nature Science Foundation of China (3071002) and the National Nature Science Foundation of China (50779070). The financial support of SNIC (the Swedish National Infrastructure for Computing) for computer time at C3SE (Chalmers Center for Computational Science and Engineering) is also gratefully acknowledged. Part of this project was financed by the EU project ATAAC (Advanced Turbulence Simulation for Aerodynamic Application Challenges), Grant Agreement No. 233710.

References

Abe, K., Kondoh, T. and Nagano, Y. (1994), A new turbulence model for predicting fluid flow and heat transfer in separating and reattaching flows – I. Flow field calculations, *Int. J. Heat Mass Transfer*, Vol. 37, pp. 139-151.

Basu, D., Hamed, A. and Das, k. (2007), Assessment of partially averaged Navier-Stokes (PANS) multiscale model in transonic turbulent separated flows, In: 5th Joint ASME/JSME Fluids Engineering Conference. July 30-August 2, San Diego, California USA.

Davidson, L. and Peng, S.-H. (2003), Hybrid LES-RANS: A one-equation SGS Model combined with a $k-\omega$ model for predicting recirculating flows, *Int. J. Numerical Methods in Fluids*, Vol. 43, pp. 1003-1018.

Emvin, P. (1997), The full multigrid method applied to turbulent flow in ventilated enclosures using structured and unstructured grids, PhD thesis, Dept. of Thermo and Fluid Dynamics, Chalmers University of Technology, Göteborg.

Fröhlich, J., Mellen, C., Rodi, W., Temmerman, L. and Leschziner, M.A. (2005), Highly-resolved large eddy simulations of separated flow in a channel with streamwise periodic constrictions, *J. Fluid Mech.*, Vol. 526, pp. 19-66.

Girimaji, S.S. (2006), Partially-averaged Navier-Stokes model for turbulence: A Reynolds-averaged Navier-Stokes to direct numerical simulation bridging method, *ASME J. Applied Mechanics*, Vol. 73, pp. 413-421.

Girimaji, S.S. and Lavin, T.A. (2007), Investigation of turbulent square jet using PANS method, AIAA Paper 5860-5870.

Hoyas, S. and Jimenez, J. (2008), Reynolds number effects on the Reynolds-stress budgets in turbulent channels, *Physics of Fluids*, Vol. 20, No. 101511.

Menter, F., Kuntz, M. and Bender, R. (2003), A scale-adaptive simulation model for turbulent flow simulation, AIAA Paper 2003-0767.

Nagano, Y. and Tagawa, M. (1990), An improved form of the $k-\varepsilon$ model for boundary layer flows, *J. Fluids Engineering.*, Vol. 112, pp. 33-39.

Spalart, P.R., Jou, W.-H., Strelets, M. and Allmaras, S. R. (1997), Comments on the feasibility of LES for wings and on a hybrid RANS/LES approach, In C. Liu and Z. Liu, editors, *advances in LES/DNS, First Int. Conf. on DNS/LES*, Louisiana Tech University, Greyden Press.